A study of the optical resonances of various nanostructured silver systems with cylindrical symmetry

J. L. García-Romero[a], T. Mendívil-Reynoso[a], E. Samano-Hermosillo[b], J. Montaño-Peraza[a,*], L. P. Ramírez-Rodríguez[a]

[a] *Department of Physics, University of Sonora, Calle Rosales y Blvd. Luis Encinas Johnson S/N, C.P. 83000, Hermosillo, Sonora, Mexico*

[b] *Industrial Engineering Educational Program, State University of Sonora, Hermosillo Academic Unit, Av. Ley Federal del Trabajo and Calle Israel González S/N, C.P. 83100, Hermosillo, Sonora, Mexico*

In the present work, the optical resonances of different silver nanoparticle systems with cylindrical symmetry are studied by using the COMSOL Multiphysics® professional package. The purpose of the research is to analyze the dependence of optical resonances on the geometry. We found a strong dependence between plasmons and geometry.

(Received December 23, 2021; Accepted April 7, 2022)

Keywords: COMSOL Multiphysics, Drude model, Plasmon, Nanostructures

1. Introduction

The capability of free electrons in metal nanoparticles to oscillate in response to electromagnetic waves produces collective oscillations that are known as surface plasmons [1]. The resonance frequency of surface plasmons depends on the size and shape of the nanoparticles, the local environment, and the material itself. *Plasmonics* is the branch of Physics that explores how the electromagnetic fields can be confined over dimensions smaller than the wavelength [2]. Plasmon resonances allow for the enhancement and manipulation of local electromagnetic fields at the nanoparticle surfaces. There are several theoretical approaches to analyze the optical response of metal nanoparticles depending on their shape. The Mie theory [3], which is an exact solution of light scattering by a sphere, accurately reproduces the optical properties of diverse metallic nanoparticles with spherical geometry. The quasi-static approximation is another analytical theory in which the Laplace equation is solved by using a frequency dependent dielectric function. This approximation can be applied to metal nanoparticles with arbitrary shape. On the other hand, some numerical methods, such as discrete dipole approximation (DDA) [4–9], the finite element method (FEM) [10,11], and the finite difference time domain (FDTD) take advantage on the currently available computing resources to solve the plasmon characteristics of metal nanoparticles with more complex geometries, including core-shell nanostructures [12–14]. The plasmon hybridization method was used to study concentric nano-shell and dimers [15,16]. Moradi studied various configurations of systems with cylindrical symmetry [17–19]; these interesting studies are based on in the quasi-static approximation and the addition theorem for Bessel function.

It is important to mention that the interaction of radiation with matter is studied by the dielectric function, which depends on the angular frequency; this kind of material is called *dispersive*. In many works, the Drude model is considered to approximate the dielectric function of metallic nanoparticles. Due to the large availability of synthesis process of metal nanoparticles, the interest on Plasmonics has increased in the last few years. Most of the research related with Plasmonics has been focused on silver and gold nanoparticles due to their interesting optical properties and wide potential applications. The plasmon resonance of round-shaped nanoparticles of silver and gold with sizes around 10 nm has been reported in the visible region, around 380 [20]

[*] Corresponding author: javier.montano@unison.mx
https://doi.org/10.15251/JOR.2022.182.239

and 520 nm [21], respectively. The dependence of the plasmon characteristics on the local environment surrounding the metal nanoparticles has been used for chemical and biological sensing applications. Another application for plasmons is the surface-enhanced Raman spectroscopy phenomena (SERS). SERS effect appears due to two mechanisms: an electromagnetic mechanism (plasmon) and a chemical mechanism. SERS that use silver and gold nanoparticles are employed for the detection of pollutants [22], biomolecules, bacteria [23], and cancer cells [24]. Other important examples in which SERS was employed are the reports by Beier *et al.* [25] and Premasiri *et al.* [26]; Beier *et al.* [25] studied β-amyloid peptide using gold nano-shells as the substrate, whereas Premasiri *et al.* [26] studied human blood using gold nanoparticles and silicon dioxide (SiO_2) as the substrate.

In the present work, we determine the surface plasmon resonances of silver nanoparticles in vacuum and water media. For this, we employed the COMSOL Multiphysics® package and a quasi-static model developed by Moradi along the Drude model for the dielectric function. Different systems composed of silver nanoparticles were studied here and the resonances were found to be in the visible spectrum with good agreement with the experimental values reported in literature.

2. Theory

One of the systems that we studied here corresponds to the optical modes of a metal single cylinder of radius r. The transcendental equation for the optical modes associated with this cylinder structure is given by the following equation [27]:

$$\beta I'_m(\eta r)H_m^{(1)}(\beta r) + \eta I_m(\eta R){H'}_m^{(1)}(\beta r) = 0 \tag{1}$$

where $\beta = \sqrt{\varepsilon_0\omega^2/c^2}$, $\eta = \sqrt{-\varepsilon(\omega)\omega^2/c^2}$, $H_m^{(1)}(\beta r)$ is the Hankel function, and $I_m(\eta r)$ is the modified Bessel function, the prime means the total. In this article, we consider that the nanostructures behave like in the Drude model, that is, the dielectric permittivity is:

$$\varepsilon(\omega) = \varepsilon_\infty - \frac{\omega_p^2}{\omega(\omega+i\gamma)} \tag{2}$$

where ε_∞ and γ at account for the permittivity at high frequencies and the collision frequency, respectively, while $\omega_p$is the bulk plasma frequency. By considering the limit for small radii (about 10 nm), the solution of the dispersion relation is ($\omega_s$is the resonance plasmon frequency)[27]:

$$Re[\omega] = \sqrt{\omega_s^2 - \frac{\gamma^2}{4}}\,, \tag{3}$$

and

$$Im[\omega] = -\gamma/2\,, \tag{4}$$

By using the Drude model, with $\gamma^2 \ll \omega_p^2$, then

$$Re[\omega] = \frac{\omega_p}{\sqrt{1+\varepsilon_\infty}}\,. \tag{5}$$

On the other hand, one of the results of Moradi for the nanotube structure [18], when the longitudinal wave vector is zero, is the following:

$$\omega_{\pm}^2 = \frac{\omega_p^2}{2}\left[1 \pm \left(\frac{r_1}{r_2}\right)^m\right]. \tag{6}$$

The latter equation is useful to calculate the resonances for a nanotube structure (that is, a nanotube cylindrical structure), where r_1 is the internal radius (radius of the aperture) and r_2 the external radius (the shell radius, that it, from the center to the nanotube periphery). Moradi solved the Laplace equation, whose radial solution concerns modified Bessel functions, and by applying the boundary conditions, he found the resonance frequencies—the plasmons.

For the non-concentric nanotube structure (that is, a non-concentric core shell cylindrical structure), it is useful the addition theorem for modified Bessel functions to evaluate the boundary conditions due to a broken symmetry [18]. For some considerations, the resonances are:

$$\omega_{\pm}^2 = \frac{\omega_1^2+\omega_2^2}{2} \pm \sqrt{\left(\frac{\omega_1^2-\omega_2^2}{2}\right)^2 - \omega_p^4 q a_1 q a_2 I_0^2(qd) K_0(qr_1) K_0'(qr_1) I_0(qr_2) I_0'(qr_2)}\,, \tag{7}$$

where $\omega_1^2 = \omega_p^2 I_m'(qr_1) K_m(qr_1)$, $\omega_2^2 = -\omega_p^2 K_m'(qr_2) I_m(qr_2)$, $K_m(qr_1)$ is the Kelvin function, the prime means the total derivate and q is the longitudinal wave vector. Here, the parameter of distance between the axis of each cylinder is d. In a similar way, for the case of two parallel cylinders along to the z axis (a pair of nanorods), the equation of the resonant frequencies is [28]:

$$\omega_{\pm}^2 = \frac{\omega_{nanorod-1}^2+\omega_{nanorod-2}^2}{2} \pm \sqrt{\left(\frac{\omega_{nanorod-1}^2-\omega_{nanorod-2}^2}{2}\right)^2 + \omega_p^4 (\kappa r_1)^4 [K_0(\kappa d) I_0(\kappa r_1) I_0(\kappa r_1)]^2}\,. \tag{8}$$

where $\kappa^2 = q^2 - \frac{\omega^2}{c^2}$; if the distance between the centers of the two nanorods is theoretically infinite, the optical behavior of the system is as if it were a single nanorod, this means $\omega_{\pm} = \omega_{nanorod} = \frac{\omega_p}{\sqrt{1+\varepsilon_\infty}}$

In this work, we used the COMSOL Multiphysics® software in order to calculate the scattering cross section per unit length (C_{scat}), the absorption cross section per unit length (C_{abs}), and the sum of both, called extinction cross section per unit length (C_{ext}), with the aim of obtaining the plasmons. COMSOL Multiphysics® software uses the finite element method. Is it important to point out the following two considerations: (1) the studied systems correspond to a cylindrical symmetry (that is, assuming that cylinder length is infinite, which leads to the use of longitude units instead of area units); and (2) the Drude model is the operative one. These considerations permit to work with a realistic material besides saving time for computational calculus.

3. Results and discussion

The following texts is divided in two subsections to properly address each of the studied cylindrical configurations. The first subsection is for single-cylinder systems, in which the nanorod and different nanotube configurations are included. The second subsection is for a two-cylinder system, namely, a pair of nanorods. Figure 1 aims to help the reader about the different configurations studied in the present research.

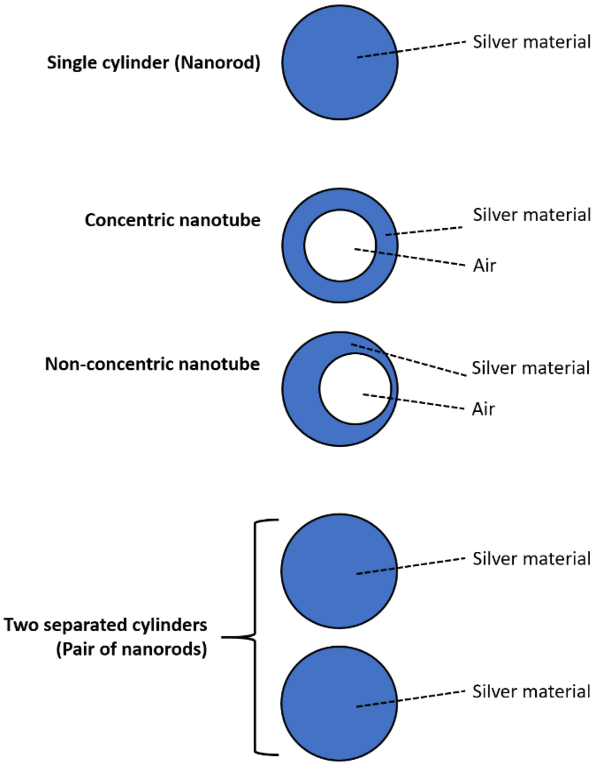

Fig. 1. Cylindrical configurations studied in the present research.

3.1. Single-cylinder systems

3.1.1. Nanorods

The first system addressed in this work is a single non-hollow silver cylinder with a radius of 5.0 nm (nanorod), in which we applied an incident plane wave with transversal-electric (TE) polarization, that is, $\vec{H} = \vec{H}_0 e^{-ikx}$, by setting the electric field oscillating in the y axis; the modulus of the electric field for this case is shown in the Figure 2. Since the electric field of the incident plane wave oscillates in y axis, then the electrons of the material will vary along of the same y direction; therefore, this induce the modulus of the electric field to have its maximum intensities along the y direction.

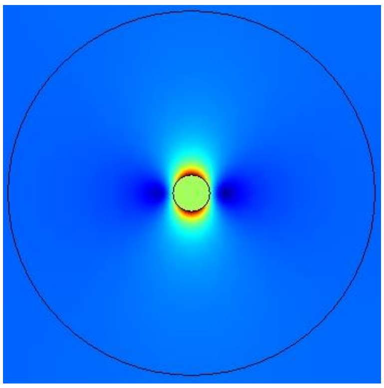

Fig. 2. Modulus of the electric field for the wavelength of 360 nm, for a cylinder with radius of 5.0 nm.

The calculated extinction cross section as a function of wavelength is shown in Figure 3, in which the resonance is appreciated at about 335.4 nm. This result is consistent with that reported in Ref. [27], in which the resonance is around 3.7 eV (that is, 335 nm).

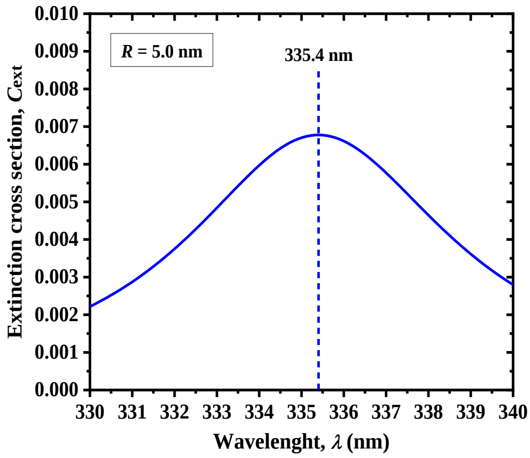

Fig. 3. Extinction cross section as a function of the wavelength for a cylinder with a radius of 5.0 nm.

As resonances depend on radius, in Figure 4 we present the calculated extinction cross section values for the single cylinder structure having different radii: 5.0, 7.5, and 10.0 nm. Here, it is observed that as the radius of the cylinder increases, there is a redshift from 335.4 to 336.9 nm, thus confirming that the optical behavior is modified depending on the cylinder size. It is important to note that although its resonance varies, the non-retarded approximation is consistent for a radius of around 5 nm.

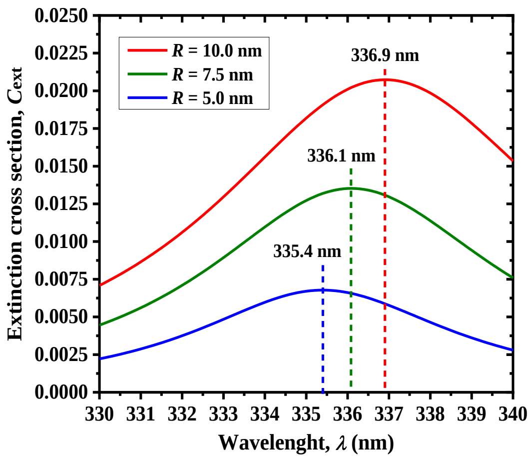

Fig. 4. Extinction cross section as a function of the wavelength for the cylinder structure with different radii: 5.0, 7.5, and 10.0 nm.

3.1.2. Concentric nanotube by Drude model

The radii, electrical permittivity ($\varepsilon(\omega) = 1 - \frac{\omega_p^2}{\omega^2}$) and plasma frequency ($\frac{h}{2\pi}\omega_p = 8.03eV$,) are the same as Moradi's work, with the only difference that the present work uses the finite element method and Moradi uses the non-retarded approximation,

$$\omega_{\pm}^2 = \frac{\omega_p^2}{2}\left[1 \pm \left(\frac{r_1}{r_2}\right)^m\right]. \tag{9}$$

Once the calculations made with COMSOL are validated, the dielectric permittivity is modified to study the silver nanostructures. For m ≠ 0, substituting values (r1 = 5.0 nm and r2 = 8.0 nm) gives two plasmons located at 171 and 356 nm. On the other hand, when using COMSOL (the Finite Element Method), the two plasmons resulted at 172 and 359 nm. This represents an error of less than 1% with respect to the theoretical result, thus showing that the methodology is valid and reliable. The modulus of the electric field of the concentric and non-concentric nanotube is shown in Figures 5 and 6 respectively.

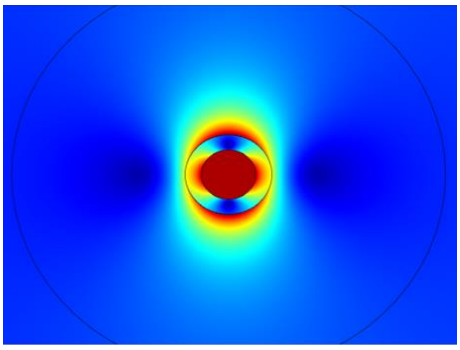

Fig. 5. Modulus of the electric field for 400 nm wavelength for the concentric nanotube. The r_1 and r_2 of the nanotube are 5.0 and 8.0 nm, respectively.

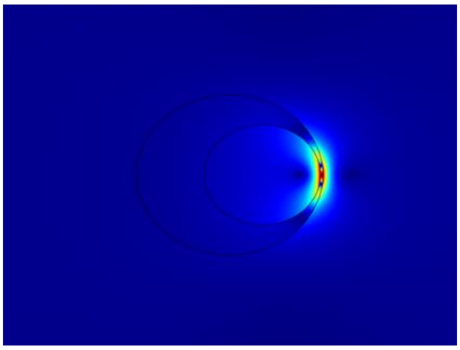

Fig. 6. Modulus of the electric field for the 400 nm wavelength for the non-concentric nanotube. The r_1 and r_2 of the nanotube are 5.0 and 8.0 nm, respectively, and the center separation is 2.8 nm.

3.1.3. Concentric and non-concentric nanotubes

In the present subsection, we present the study on different non-concentric nanotube configurations by considering the model by Nápoles et al. [27] (described in the Theory section); we also include here the analysis performed on concentric nanotubes. The behavior of light interacting with different concentric nanotube configurations will be also studied; in this regard, Figure 7 shows the extinction cross section for different internal and external radii. It is observed here that there are two resonances for the nanotube structures, independently of the radius value. Also, as the relation between the external and internal radius is lower, the separation and the intensity ratio between both resonances is increased, that is, the resonance at the lowest frequency is displaced more to the right (to the red) and increases in intensity, while the resonance at the higher frequency is displaced more to the left (to the blue) and decreases in intensity. In the case of $r_1 = 0$ and $r_2 = 8\,nm$ (a nanorod) the plasmon frequency converges to 336 nm which is the plasmon resonance in the non-retarded approximation.

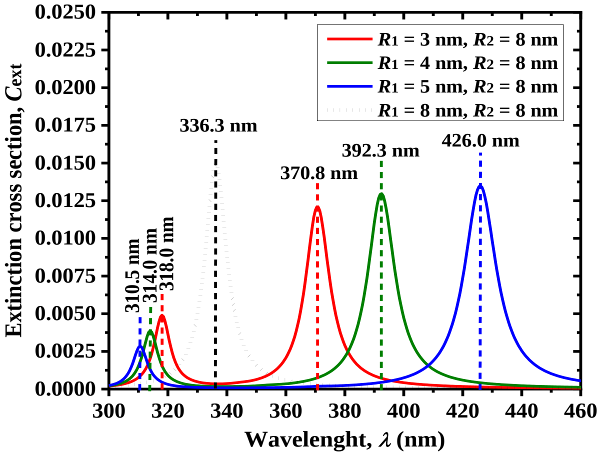

Fig. 7. Extinction cross section as a function of wavelength for a concentric nanotube structure for different radius configurations.

On the other hand, Figure 8 shows the results on non-concentric nanotubes with different center separation values (d), with $r_1$and r_2 equal to 5 nm and 8 nm. We observed here a red shift of the resonances as the parameter d increases, which was also noted by Moradi [17]. In Figure 9 we show the modulus of the electric field for the particular case of the non-concentric nanotube structure with r_1 = 5.0 nm, r_2 = 8.0 nm, and d = 1.5 nm, as calculated for a wavelength of 440 nm.

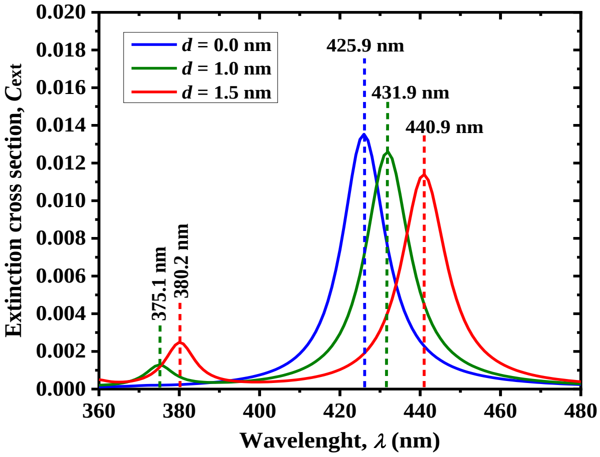

Fig. 8. Extinction cross section as a function of wavelength for a non-concentric nanotube for different distances between the centers of the cylinders configurations.

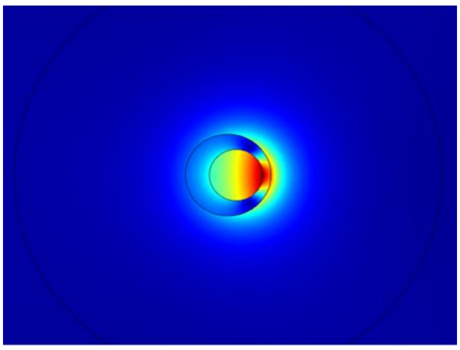

Fig. 9. Modulus of the electric field for the 440 nm wavelength. The r_1, r_2, and d of the non-concentric nanotube are 5.0 nm, 8.0 nm, and 1.5 nm, respectively.

With the aim of studying the symmetry with respect to the θ angle, three calculations were made by fixing the center separation at 1.5 nm: (x = -1.5 nm, y = 0), (x = 1.5 nm, y = 0), and (x = 0, y = 1.5 nm).

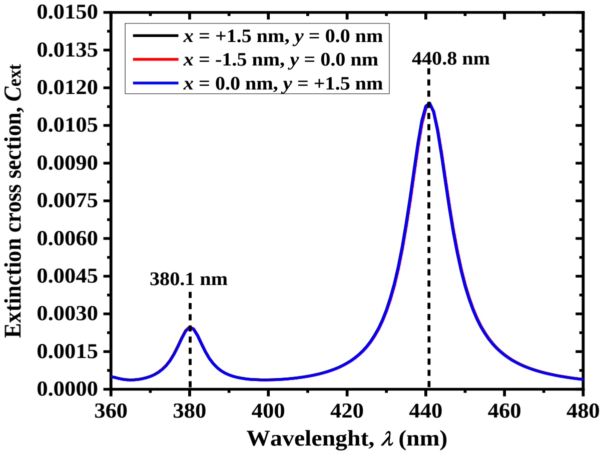

Fig. 10. Extinction cross section with respect to wavelength for a non-concentric nanotube cylinder for different configurations. The r_1, r_2, and d of the non-concentric nanotube are 5.0 nm, 8.0 nm, and 1.5 nm, respectively.

The first conclusion, as shown in Figure 10, is that the symmetry does not vary. However, when studying the case of (x = 1.5 nm, y = 1.5 nm), the symmetry was broken, as shown in Figure 11. But, when the studied values are (x = -1.5 nm, y = 1.5 nm), (x = 1.5 nm, y = 1.5 nm) and (x = -1.5 nm, y = -1.5 nm), we observed that the symmetry is maintained constant again, as shown in Figure 12. From these observations, we concluded that the C_{ext} depends only on the center separation.

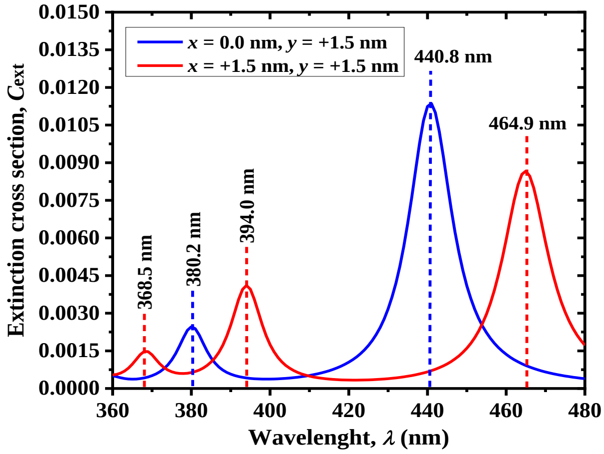

Fig. 11. Extinction cross section as a function of wavelength for a non-concentric nanotube cylinder for different configurations. The r_1, r_2 of the non-concentric nanotube are 5.0 nm and 8.0 nm, respectively, the distance between the center of the cylinder d are 1.5 (blue line) and $\sqrt{4.5}$ (red line) nm.

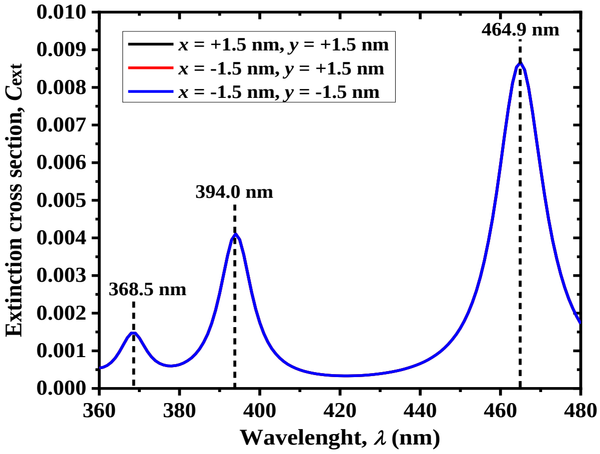

Fig. 12. Extinction cross section with respect to wavelength for a non-concentric nanotube cylinder for different configurations. The r_1, r_2, and d of the non-concentric nanotube are 5.0 nm, 8.0 nm, and $\sqrt{4.5}$ nm, respectively.

The first two-cylinder system that we studied here corresponds to two cylinders with radii of 5.0 nm each, with a separation between them of 1.0, 5.0, 10.0, 20.0, and 40.0 nm, using an arrangement where the cylinders are next to each other and parallel to the horizontal, and with the magnetic field incident along the x axis, that is, with $\vec{H} = \vec{H}_0 e^{-ikx}$. Figure 13 shows the modulus of the electric field for the cases in which the separation is 1.0, 5.0, and 40.0 nm, as examples. In Figure 14 we can see that the shorter the distance between the two cylinders the greater the number of produced resonances; this is understandable, since the shorter the distance between the two cylinders the greater the interaction between them. For example, three resonances appear with just 1.0 nm of separation, but it is reduced to two resonances when the distance is increased to 5.0 nm; just one resonance is obtained with the separation values of 10.0, 20.0, and 40.0 nm. In conclusion, when the magnetic field incident is along the x axis, a longer distance between the two cylinders leads to a smaller interaction between them and, thus, a smaller number of resonances, which, in turn, are more intense and more displaced to the red.

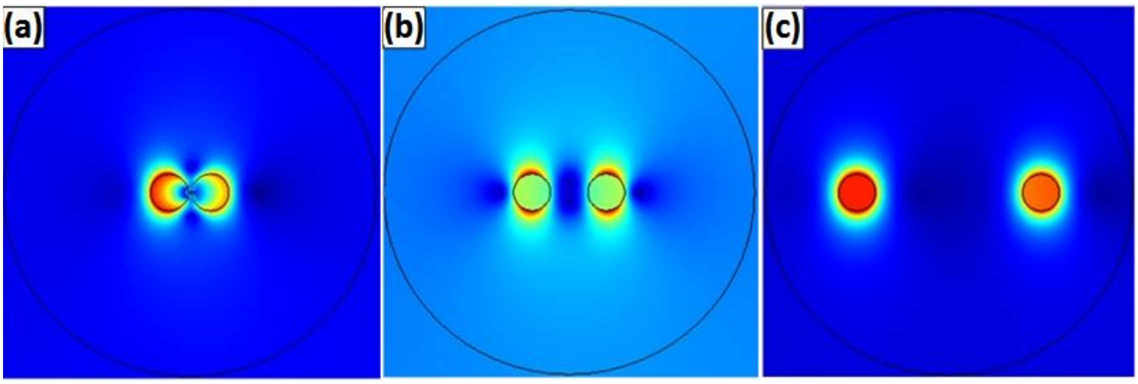

Fig. 13. Modulus of the electric field for the wavelength 340 nm, for the two-cylinder system with radius of 5.0 nm each, with a separation between them of (a) 1.0 nm, (b) 5.0 nm, and (c) 40.0 nm. The magnetic field incident is along the x axis.

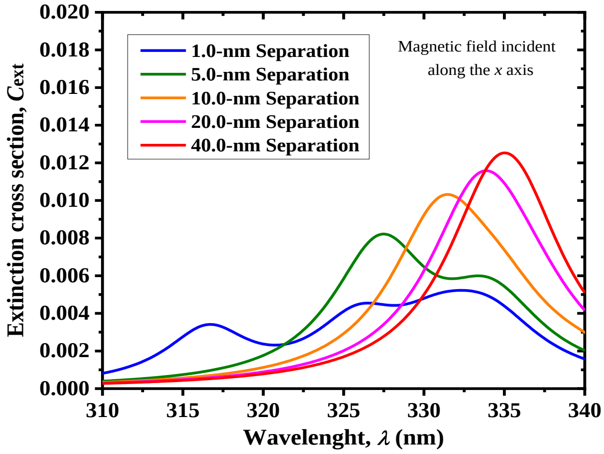

Fig. 14. Extinction cross section as a function of the wavelength for the two-cylinder system with radius of 5.0 nm each, with different separation values between them. The magnetic field incident was along the x axis.

The second two-cylinder system that we studied is similar to the previous one, but with the magnetic field incident along the y axis, that is, with $\vec{H} = \vec{H}_0 e^{-iky}$. Figure 15 shows the modulus of the electric field for the cases in which the separation is 1.0, 5.0, and 40.0 nm, as examples.

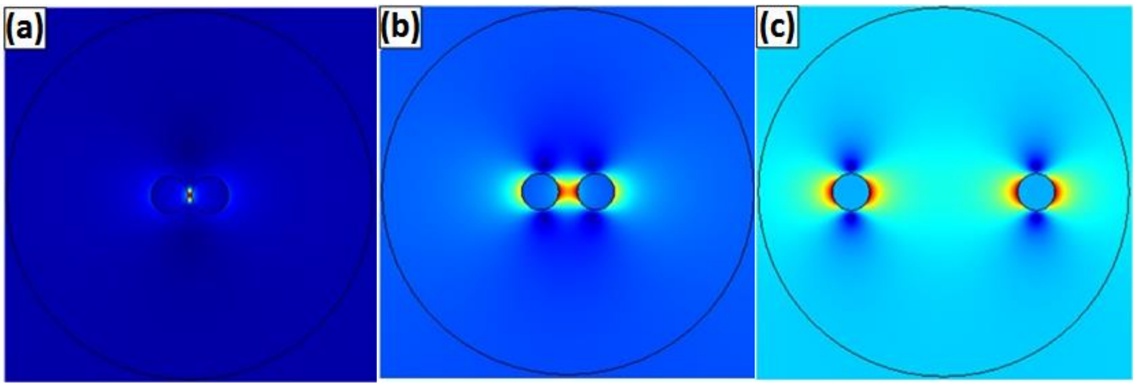

Fig. 15. Modulus of the electric field for the wavelength 400 nm, for the two-cylinder system with radius of 5.0 nm each, with a separation between them of (a) 1.0 nm, (b) 5.0 nm, and (c) 40.0 nm. The magnetic field incident is along the y axis.

In Figure 16 we can see that the shorter the distance between the two cylinders the greater the number of produced resonances, which is due to a higher interaction between them. This result is consistent with the previous case, where the magnetic field incident was at the x axis. However, for the present case, where the magnetic field incident is at the y axis, the resonances are displaced to the blue instead to red as the distance between the cylinders is longer. This is the main difference between both cases.

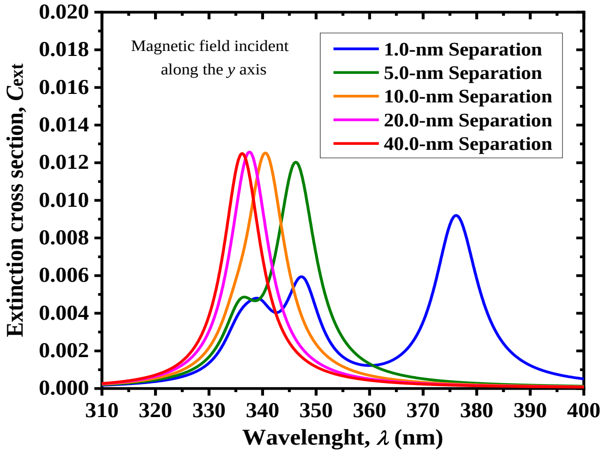

Fig. 16. Extinction cross section as a function of the wavelength for the two-cylinder system with radius of 5.0 nm each, with different separation values between them. The magnetic field incident was along the y axis.

4. Conclusions

The behavior of light when interacting with silver nanotube structures was resolved by using the finite element method. An interesting result was observed when varying the radius of a single non-hollow cylinder (nanorod): a redshift and an increase of the extinction section were observed as the radius of each cylinder increases. This result means that the optical response of the material strongly depends on the geometry.

For the nanotube case, it was observed a redshift of the resonance as the ratio between the external radius and the internal radius increases, and the symmetry depends only on the distance between the centers. For the present case, we observed two main results. First, when there is an offset of the arrangement only in the horizontal or only in the vertical axis, by keeping fixed the distance between the centers, the resonances that we find are the same (the symmetry is maintained); the following coordinates are clear examples: (x = 1.5, y = 0), (x = -1.5, y = 0) and (x = 0, y = 1.5). Second, when we make an offset on both the vertical and horizontal axis, the symmetry is lost as compared with the cases in which there was only an offset in one axis. However, the symmetry is recovered again if the distance between the centers is maintained, as in the following coordinates: (x = 1.5, y = 1.5), (x = -1.5, y = -1.5), and (x = -1.5, y = 1.5. Therefore, we conclude that resonance only depends on the distance between the centers of both cylinders (cylinders with fixed radii).

When studying the case involving a pair of nanorods (two cylinders), it is observed that the separation between the cylinders affects the optical properties due to the change in the electromagnetic interaction between them. However, for the case where the separation between them is around 40 nm, the two-cylinder system behaves as a single nanotube. We also found that the plasmons depended on the way in which the field was affected, that is, it is different if it is affected by $\vec{H} = \vec{H}_0 e^{-iky}$ or $\vec{H} = \vec{H}_0 e^{-ikx}$.

Acknowledgements

With special acknowledged to Geovanna Navarrete Romero for the translation support, and Jorge Garcia Valenzuela for the contribution and participation in this work.

References

[1] U. Kreibig, M. Vollmer, Optical Properties of Metal Clusters, Springer-Verlag Berlin Heidelberg, 9, 1995; https://doi.org/10.1007/978-3-662-09109-8.
[2] S. A. Maier, Plasmonics: Fundamentals and Applications, Springer US, xxiii 2007 https://doi.org/10.1007/0-387-37825-.
[3] G. Mie, Annalen der Physik 330(3) (1908) 377; https://doi.org/10.1002/andp.19083300302
[4] E.M. Purcell, C.R. Pennypacker, The Astrophysical Journal 186 (1973) 705; https://doi.org/10.1086/152538.
[5] B.T. Draine, P.J. Flatau, User guide for the discrete dipole approximation code DDSCAT 7.3, arXiv:1305.6497, last revised: 2013 May 26.
[6] B.T Draine, P.J. Flatau, Journal of the Optical Society of America A 11(4) (1994) 1491; https://doi.org/10.1364/JOSAA.11.001491.
[7] C. Noguez, The Journal of Physical Chemistry C 111(10) (2007) 3806; https://doi.org/10.1021/jp066539m.
[8] K.L. Shuford, M.A. Ratner, G.C. Schatz The Journal of Chemical Physics 123(11) (2005); https://doi.org/10.1063/1.2046633.
[9] J. Boneberg, J. König-Birk, H.-J. Münzer, P. Leiderer, K.L. Shuford, G.C. Schatz, Applied Physics A 89 (2007) 299; https://doi.org/10.1007/s00339-007-4138-y.
[10] M.W. Knight, N.J. Halas New Journal of Physics 10 (2008) 105006; https://doi.org/10.1088/1367-2630/10/10/105006.
[11] J. Zhao, A.O. Pinchuk, J.M. McMahon, S. Li, L.K. Ausman, A.L. Atkinson, G.C. Schatz Accounts of Chemical Research 41(12) (2008) 1710; https://doi.org/10.1021/ar800028j.
[12] B. Butrylo, C. Vollaire, L. Nicolas IEEE Transactions on Magnetics 40(2) (2004) 1424; https://doi.org/10.1109/TMAG.2004.825426.
[13] J.M. McMahon, J. Henzie, T.W. Odom, G.C. Schatz, S.K. Gray Optics Express 15(26) (2007) 18119; https://doi.org/10.1364/OE.15.018119.
[14] V. Uzayisenga, X.-D. Lin, L.-M. Li, J.R. Anema, Z.-L. Yang, Y.-F. Huang, H.-X. Lin, S.-B. Li, J.-F. Li, Z.-Q. Tian Langmuir 28(24) (2012) 9140; https://doi.org/10.1021/la3005536.
[15] E. Prodan, C. Radloff, N.J. Halas, P. Nordlander, Science 302(5644) (2003) 419; https://doi.org/10.1126/science.1089171.
[16] P. Nordlander, C. Oubre, E. Prodan, K. Li, M.I. Stockman Nano Letters 4(5) (2004) 899; https://doi.org/10.1021/nl049681c.
[17] A. Moradi, Journal of Physics and Chemistry of Solids 69(11) (2008) 2936; https://doi.org/10.1016/j.jpcs.2008.08.004.
[18] A. Moradi Optics Communications 282(16) (2009) 3368; https://doi.org/10.1016/j.optcom.2009.05.016.
[19] A. Moradi, Plasmon hybridization in tubular metallic nanostructures, Physica B: Condensed Matter 405(10) (2010) 2466; https://doi.org/10.1016/j.physb.2010.03.010.
[20] J.A. Scholl, A.L. Koh, J.A. Dionne Nature 483(7390) (2012) 421; https://doi.org/10.1038/nature10904.
[21] M. Hu, J. Chen, Z.-Y. Li, L. Au, G.V. Hartland, X. Li, M. Marquez, Y. Xia, Chemical Society Reviews 35(11) (2006) 1084; https://doi.org/10.1039/b517615h.
[22] M. Baia, V. Danciu, V. Cosoveanu, L. Baia Vibrational Spectroscopy 48(2) (2008) 206; https://doi.org/10.1016/j.vibspec.2008.03.005.
[23] W.R. Premasiri, D.T. Moir, M.S. Klempner, N. Krieger, G. Jones 2nd, L.D. Ziegler, The Journal of Physical Chemistry B 109(1) (2005) 312; https://doi.org/10.1021/jp040442n.
[24] D.S. Grubisha, R.J. Lipert, H.-Y. Park, J. Driskell, M.D. Porter, Analytical Chemistry 75(21) (2003) 5936; https://doi.org/10.1021/ac034356f.
[25] H.T. Beier, C.B. Cowan, I.-H. Chou, J. Pallikal, J.E. Henry, M.E. Benford, J.B. Jackson, T.A. Good, G.L. Coté, Plasmonics 2(2) (2007) 55; https://doi.org/10.1007/s11468-007-9027-x.
[26] W.R. Premasiri, J.C. Lee, L.D. Ziegler, The Journal of Physical Chemistry B 116(31) (2012) 9376; https://doi.org/10.1021/jp304932g.

[27] J.M. Nápoles-Duarte, M.A. Chavez-Rojo, M.E. Fuentes-Montero, L.M. Rodríguez-Valdez, R. García-Llamas, J.A. Gaspar-Armenta Journal of Optics 17(6) (2015) 065003; https://doi.org/10.1088/2040-8978/17/6/065003.
[28] A. Moradi JETP Letters 88(12) (2008) 795; https://doi.org/10.1134/S0021364008240041.